



Universitatea *Transilvania* din Braşov

## HABILITATION THESIS

### SUMMARY

**Color and Multispectral Texture Image Analysis.  
Models, Features and Applications**

**Domain: Electronics and Telecommunications  
Engineering**

**Author: Laurențiu-Mihail Ivanovici**

**University: Universitatea Transilvania din Braşov**

**BRAŞOV, 2015**



# Summary

The research work that constitutes the support for the habilitation thesis<sup>1</sup> started in 2007 in collaboration with Noël Richard from the XLIM-SIC research laboratory, Université de Poitiers, France. Along with the presentation and the emphasis of the outstanding achievements so far, in this thesis the future research paths are sketched. After a short introduction on color and multispectral texture images, the fractal models which can be used for texture modeling are discussed. The models can be used both for synthesis and analysis. Then, in the context of analysis, various texture feature extraction techniques are presented, especially the fractal and morphological<sup>2</sup> ones. In the final chapter, image segmentation and texture classification are presented as applications.

Textures represent the variation of a signal (i.e. image) at a lower scale than the one of interest [33]. Textures can be regular, semi-regular or irregular (see Fig. 1). Most natural textures are irregular. Another taxonomy classifies textures in deterministic or random.



Fig. 1: Types of textures.

The notion of texture emerged in the ‘60-’70s in the context of analysis of gray-scale images that present certain variations at object surface that rendered difficult the task of image segmentation. According to Haralick

---

<sup>1</sup>M. Ivanovici, “Color and Multispectral Texture Image Analysis – Models, Features and Applications”, Transilvania University Press, ISBN 978-606-19-0587-4, 2015, <http://miv.unitbv.ro/downloads/MIVCMTIAMFA2015.pdf>

<sup>2</sup>We talk here about the mathematical morphology - a fundamental domain for non-linear image processing and analysis. See for instance P. Soille *Mathematical morphology and image analysis*.

[18] texture can be described using terms like fine, coarse or smooth. Haralick introduced the gray-tone spatial-dependence matrices, also known as gray-level co-occurrence matrices, as a way to characterize texture. Based on these matrices he proposed 14 texture features regarding homogeneity, contrast, number and nature of boundaries, and the complexity of the image. Various texture characterization tools have been proposed since then and in [40] the existing techniques were classified as being: geometrical, statistical, image model-based methods and signal processing approaches. Several important techniques are described in [32] [13] [22] [26].

In this thesis we dedicate our attention to the notion of complexity, in the context of texture image analysis. There exist various definitions of complexity, including Kolmogorov complexity and entropy. Recently, N. Richard and myself proposed a new Technical Committee within Division 8 of CIE<sup>3</sup> entitled *Specification of Spatio-Chromatic Complexity*. Its objective is to produce a single definition of spatio-chromatic complexity embedding the spatial and chromatic variations in a generic and vector form, taking into account both spatial and spectral variations of textures, in order to propose an international standard.

For the validation of models and analysis tools for color textures various texture image databases have been constructed, some of them for the purpose of testing translation, rotation, scale and illuminant-invariant feature extraction or classification approaches. Two of the most used and well-known texture image data-bases are Outex [29] and VisTex<sup>4</sup>.

Recently, the scientific community has focused its attention to multi-spectral texture analysis. There are several databases available, one of them being CAVE<sup>5</sup>, Columbia University, New York which contains multispectral images with 31 spectral bands, from 400 nm to 700 nm, in steps of 10 nm. Several open-access multispectral image data-bases are available: University of East Anglia, United Kingdom<sup>6</sup>, Brno University of Technology, Czech Republic<sup>7</sup> or the Joint Research Center, the Institute for Environment and Sustainability<sup>8</sup>. The latter one contains Landsat 7 satellite images.

## Fractal models

Fractal geometry was introduced by B. Mandelbrot in 1983 [27] in order to describe self-similar sets called *fractals*. Self similarity is a central concept of the fractal geometry, being closely connected to the notion of dimension and implicitly to complexity. Fractal dimension is a measure of the complexity

---

<sup>3</sup>International Commission on Illumination.

<sup>4</sup><http://vismod.media.mit.edu/vismod/imagery/VisionTexture/>

<sup>5</sup><http://www.cs.columbia.edu/CAVE/databases/multispectral/>

<sup>6</sup><http://www2.cmp.uea.ac.uk/Research/compvis/MultiSpectralDB.htm>

<sup>7</sup><http://splab.cz/en/download/databaze/multispec>

<sup>8</sup><http://image2000.jrc.ec.europa.eu/DI/IM.htm>

of a fractal object. Fractal models are used to generate synthetic textures, shapes and even landscapes in computer graphics. From the plethora of algorithms we embraced the one of random fractal generation, mainly Brownian fractional noise generation. A technique for generating such noise is called *random midpoint displacement* proposed by D. Saupe in [32]

For the design of a color fractal image generator, we extended in [20] the random midpoint displacement method on gray levels to the color domain<sup>9</sup>. We chose to work in the RGB color space as it presents a cubic organization coherent with the construction of the fractal object.

For RGB color images, the increments used for moving the middle point are differences, in the sense of the Euclidean distance, between 3D vectors  $X_k$ , located in any two points  $t_1, t_2$  and  $s_1, s_2$  of the support space. The variance of these increments is:

$$\sigma_i^2 = \left( \sqrt{\sum_{k=r,g,b} (X_k(t_1, t_2) - X_k(s_1, s_2))^2} \right)^2 \quad (1)$$

$$\sigma_i^2 = \frac{[X_r(t_1, t_2) - X_r(s_1, s_2)]^2 + [X_g(t_1, t_2) - X_g(s_1, s_2)]^2 + \dots}{\dots + [X_b(t_1, t_2) - X_b(s_1, s_2)]^2} \quad (2)$$

In the hypothesis that the increments in the three RGB planes are statistically independent, i.e. the color stimuli on the three channels are not correlated, we can distribute the statistical operation to each term:

$$\sigma_i^2 = \frac{[X_r(t_1, t_2) - X_r(s_1, s_2)]^2}{\dots} + \frac{[X_g(t_1, t_2) - X_g(s_1, s_2)]^2}{\dots} + \frac{[X_b(t_1, t_2) - X_b(s_1, s_2)]^2}{\dots} \quad (3)$$

Because each of the three terms is proportional to  $\left( \sum_{i=1}^2 (t_i - s_i)^2 \right)^H$ , according to the construction of the fractal object in the original approach, we can conclude that the sum will be also proportional to the space coordinate differences:

$$\sigma_i^2 \propto 3 \cdot \left( \sum_{i=1}^2 (t_i - s_i)^2 \right)^H \propto \left( \sum_{i=1}^2 (t_i - s_i)^2 \right)^H \quad \square \quad (4)$$

We therefore demonstrated that the color model is valid for the color fractal images we generated using the RGB color space. For the implementation of the generation approach, we modified the algorithm presented in

<sup>9</sup>M. Ivanovici, N. Richard, *Fractal Dimension of Color Fractal Images*, IEEE Transactions on Image Processing, January 2011, <http://dx.doi.org/10.1109/TIP.2010.2059032>

[32] in order to work with RGB triplets. In Fig. 2 we show the color fractal images obtained, of different complexity (controlled by the value of the Hurst parameter).

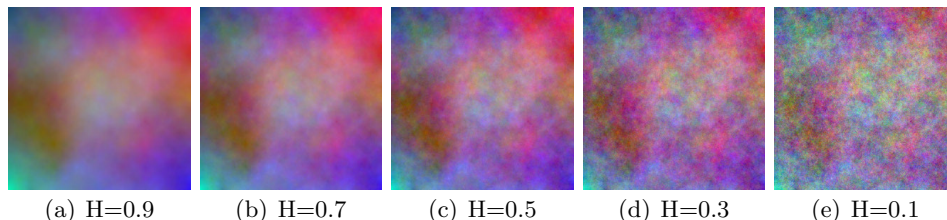


Fig. 2: Color fractal images generated in RGB.

## Fractal features

For the analysis of textures of fractal and random nature, we will focus our attention to two important fractal features: the fractal dimension and lacunarity. Fractal dimension is a measure that characterizes the complexity of a fractal, indicating the amount of irregularity and *how much* the available space is filled. Lacunarity is a complementary fractal measure which indicates *how* the space is filled, being similar to a distribution function. Fractal features are used for multi-scale image and multidimensional signals analysis by observing the variation of a measure as a function of the analysis scale.

The theoretical fractal dimension is the Hausdorff dimension [14]. In practice, this dimension is estimated either by computing the similarity dimension, the *box-counting* dimension, the correlation dimension or other dimensions. The probabilistic algorithm for estimating the box-counting dimension  $dim_B$  proposed by R. Voss [41] considers the image  $F$  as a set of points in an Euclidean space. According to [25], the spatial arrangement of the set is characterized by the probability matrix  $P(m, \delta)$  of having  $m$  points within a cube (box) of size  $\delta$ , centered in all the points of the analyzed image. For each value of  $\delta$ , the matrix is normalized so that:

$$\sum_{m=1}^Q P(m, \delta) = 1, \quad \forall \delta \quad (5)$$

where  $Q$  represents the number of points in the cubes of size  $\delta$ . If  $M$  is the total number of points of the image, the number of boxes containing  $m$  points is  $(M/m)P(m, \delta)$ . Consequently, the total number of boxes needed to cover the image is:

$$\langle N(\delta) \rangle = \sum_{m=1}^N \frac{M}{m} P(m, \delta) = M \sum_{m=1}^N \frac{1}{m} P(m, \delta) \quad (6)$$

which is an estimate of  $N(\delta)$ , so the amount  $\sum_{m=1}^Q \frac{1}{m} P(m, \delta)$  is directly proportional to  $\delta^{-\dim_B F}$  and can be used for the computation of the box-counting dimension:  $N(\delta) = \sum_{m=1}^N \frac{1}{m} P(m, \delta) \propto \delta^{-\dim_B}$ .

If a gray-level image can be modeled as a discrete surface  $z = f(x, y)$  in a three-dimensional space, where  $z$  is the luminance in every point  $(x, y)$  of the support, the model can be extended for color and multispectral images. In [20] we consider a color image as a hyper-surface in an RGB color space:  $f(x, y) = (r, g, b)$ . Therefore in the case of color images we deal with a 5-dimensional Euclidean hyper-space and each pixel can be seen as a 5-dimensional vector  $(x, y, r, g, b)$ .

The classical algorithm of Voss defines cubes of size  $\delta$  centered in the current pixel  $(x, y, z = f(x, y))$  and counts the number of pixels that fall within a cube determined by the following two opposite corners:  $(x - \frac{\delta}{2}, y - \frac{\delta}{2}, z - \frac{\delta}{2})$  și  $(x + \frac{\delta}{2}, y + \frac{\delta}{2}, z + \frac{\delta}{2})$ . A direct extension of the Voss approach to color images would count the pixels  $F = f(x, y, r, g, b)$  for which the Euclidean distance to the center of the hyper-cube  $F_c = f(x_c, y_c, r_c, g_c, b_c)$  would be smaller than  $\delta$ :

$$|F - F_c| = \sqrt{\sum_{i=1}^5 |f_i - f_{ci}|^2} \leq \delta \quad (7)$$

Given that the Euclidean distance in the RGB space does not correspond to the perceptual distance between colors, we prefer to use instead the Minkowski infinity norm:

$$|F - F_c| = \max(|f_i - f_{ci}|) \leq \delta \quad \forall i = \overline{1, 5} \quad (8)$$

Practically, for a certain square of size  $\delta$  in the  $(x, y)$  support, we count the number of pixels that fall inside a 3-dimensional RGB cube of size  $\delta$  centered in the current pixel. In Figure 3 we show three color textures (orange, psoriasis and cladonia), with the corresponding  $N(\delta)$  curves. The estimated color fractal dimensions are 2.0, 3.39 and 3.71, respectively.

The lacunarity, as defined by Voss, is based on the first and second order moments  $M(\delta)$  and  $M^2(\delta)$  computed using the probabilities  $P(m, \delta)$ :

$$M(\delta) = \sum_{m=1}^N m P(m, \delta) \quad M^2(\delta) = \sum_{m=1}^N m^2 P(m, \delta) \quad (9)$$

$$\Lambda(\delta) = \frac{M^2(\delta) - (M(\delta))^2}{(M(\delta))^2} \quad (10)$$

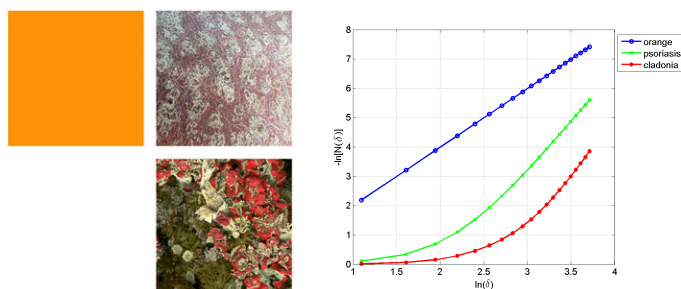


Fig. 3: Three textures and the corresponding  $N(\delta)$  curves.

Modeling the color images in the same way as for the estimation of the box-counting dimension, we obtain the following results<sup>10</sup> presented in Fig. 4: the lacunarity curves for three of the color fractal images in Fig. 2 and the textures in Fig. 3.

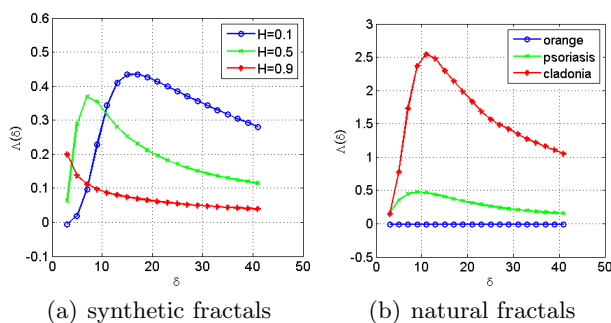


Fig. 4: Lacunarity curves.

As expressed by Mandelbrot, the interpretation of the lacunarity curves is related to the perception of *mounts* and *valleys* in the hyper-surface complexity of the texture.

## Morphological features

The domain of mathematical morphology was founded by G. Matheron [28] and J. Serra [36] and constitutes a mathematical framework for nonlinear image processing and analysis. Mathematical morphology was introduced for binary images, the basic morphological operators being based on set theory [16]. The mathematical morphology extension to gray-scale images

<sup>10</sup>M. Ivanovici, N. Richard, The lacunarity of colour fractal images, 16th IEEE International Conference on Image Processing, 2009, <http://dx.doi.org/10.1109/ICIP.2009.5414394>

is based on lattice theory, which implies a partial ordering of the image data, such that an *infimum* and a *supremum* exist for any subset of pixel values. Applications of mathematical morphology include filtering, segmentation or texture analysis [38].

The extension of mathematical morphology to color and multispectral images is not straightforward because of the vector image data, and consequently because of the need to define a suitable ordering for vector data. Ordering schemes for vector data have been classified in four groups [4]: marginal, reduced, conditional and partial, each having its advantages and disadvantages, depending on their outcome with respect to the application.

Various approaches have been proposed for color and multispectral images [3]. In parallel with developing such approaches, which respect all the properties of mathematical morphology, several *pseudo-morphologies* were proposed. These frameworks do not require an underlying ordering of the image data: instead they focus on computing the two extrema of a given set [17] [2] [7].

In [19] we proposed the estimations of the extrema of a set, the *infimum* and *supremum*, by using the Chebyshev inequality, which allows estimating the probability of a subset of vectors to belong to an interval centered around the mean of the distribution [11]. Let  $\xi$  be a random variable with mean  $\mu_\xi$  and standard deviation  $\sigma_\xi$ , then the Chebyshev inequality states that:

$$P\{|\xi - \mu_\xi| \geq k\sigma_\xi\} \leq \frac{1}{k^2} \quad (11)$$

Eq. (11) stands for any distribution with finite mean and standard deviation [30]. Using the  $k$  parameter, one may generate symmetric intervals around the mean, with the two extrema being relatively close to the real minimum or maximum values. Consequently we define the probabilistic pseudo-extrema of a distribution,  $\mathcal{E}^+$  and  $\mathcal{E}^-$ , as specified by Chebyshev inequality:

$$\begin{cases} \mathcal{E}^+ \triangleq \mu_\xi + k\sigma_\xi \\ \mathcal{E}^- \triangleq \mu_\xi - k\sigma_\xi \end{cases} \quad (12)$$

By choosing an appropriate value for  $k$ , the error between the probabilistic extrema and the real extrema of a distribution can be reduced as desired. Based on this approach, in [7] we proposed a probabilistic pseudo-morphology (PPM) for gray-scale images, further extended to the color image domain<sup>11</sup>. Given an image  $f : \mathcal{D}_f \rightarrow \mathcal{S} \subset \mathbb{R}$ , and a flat structuring element  $g$  having the support  $\mathcal{D}_g$ , we defined the pseudo-erosion and pseudo-dilation operations as follows:

<sup>11</sup>A. Căliman, M. Ivanovici, N. Richard, Probabilistic pseudo-morphology for gray-scale and color images, Pattern Recognition, ISSN 0031-3203, February 2014, <http://dx.doi.org/10.1016/j.patcog.2013.08.021>

$$[\varepsilon_g(f)](x) = \bigwedge_{z \in \mathcal{D}_g} f(x+z) \triangleq \mu_\xi - k\sigma_\xi, \quad \forall x \in \mathcal{D}_f \quad (13)$$

$$[\delta_g(f)](x) = \bigvee_{z \in \mathcal{D}_g} f(x-z) \triangleq \mu_\xi + k\sigma_\xi, \quad \forall x \in \mathcal{D}_f \quad (14)$$

where  $\xi$  represents a random variable which models the gray level of pixels falling within  $\mathcal{D}_f \cap \mathcal{D}_g$ . The mean  $\mu_\xi$  and the standard deviation  $\sigma_\xi$  are computed locally, within a neighborhood given by the size and position of the structuring element. For small  $k$  values (0.2), the probabilistic pseudo-extrema are close to the mean value and consequently the behavior of the PPM operations is similar to a smoothing filter (see Fig. 5 and 6). For  $k = 2$ , an optimum value for Lenna image, the results are similar with the ones obtained when using the classical morphological operators for gray-scale images (GLMM). Some differences occur, naturally: the classical morphology introduces artifacts (e.g. top of the hat). Due to the intrinsic statistical filtering of PPM, the resulting pseudo-eroded image does not exhibit such artifacts, the shape of the SE not being visible. In addition, PPM is capable of preserving morphological details (e.g. eyebrows) and texture (e.g. hat feathers). All these prove that PPM is less influenced by noise, the morphological or textural structures being better preserved. For a large value of  $k = 4$ , the probabilistic extrema are far away from the local mean, being pushed towards black and white, the extrema of gray-scale. This case can be similar to classical morphology using non-flat structuring elements.

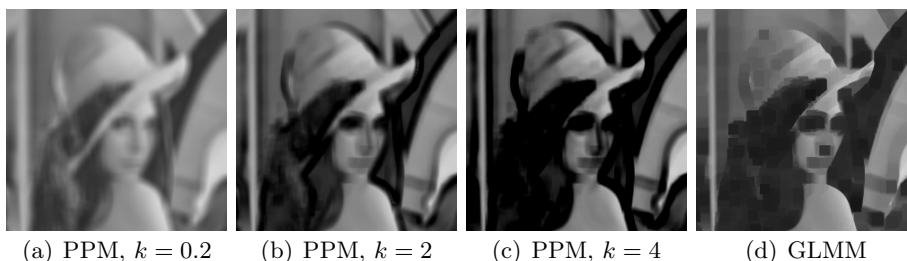


Fig. 5: PPM erosions for various values of  $k$  compared to GLMM, both using a flat structuring element of size  $11 \times 11$ .

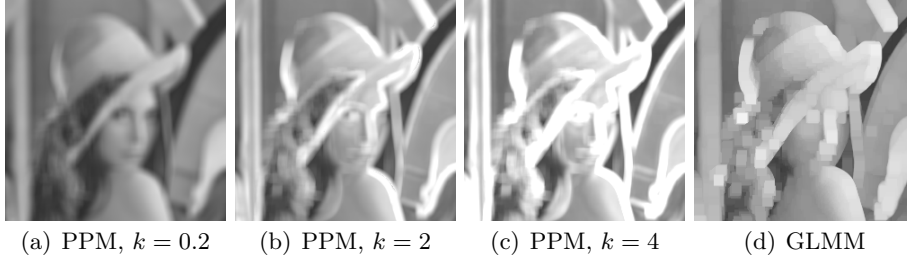


Fig. 6: PPM dilations for various values of  $k$  compared to GLMM, both using a flat structuring element of size  $11 \times 11$ .

For color images the pixel values are vectors, the images being modeled as  $f : \mathcal{D}_f \rightarrow \mathcal{S} \subset \mathbb{R}^3$ . In order to extend PPM to the color domain, we need to correctly evaluate the variance of the data, for the purpose of using the same Chebyshev inequality. In [7] we proposed a color approach based on principal component analysis (PCA). PCA is a linear transformation of the data set which identifies a new space, i.e. a set of orthogonal directions, so that the variance is maximized on one of those directions [31]. The directions of the transformed space are the eigenvectors of the covariance matrix. In Figure 7 the construction of the probabilistic pseudo-extrema is illustrated (on the first and on both principal components) in case of bi-dimensional vectors.

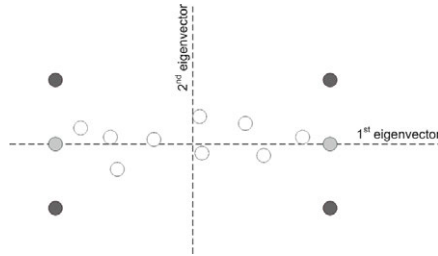


Fig. 7: Computing probabilistic pseudo-extrema of a bi-dimensional data set (white dots): using the first principal component (light gray dots) or using the two principal components (dark gray dots).

After applying PCA and the Chebyshev inequality there is still an issue to solve, due to the vector nature of data: the two extrema have to be ordered and labeled as minimum and maximum. In [7] we ordered the pseudo-extrema constructed on the first principal component using three pairs of three-dimensional reference points with an *a priori* order imposed or chosen for each pair. The ordering is performed using the projections of the pseudo-extrema on the direction determined by the reference points. This process is depicted in Figure 8, where the considered *a priori* ordering

for the reference points is  $R^+ > R^-$  and consequently the pseudo-extrema  $E_\alpha$  and  $E_\beta$  will be ordered as  $E_\alpha > E_\beta$ .

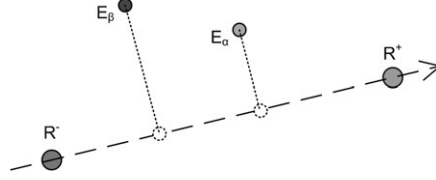


Fig. 8: Ordering  $E_\alpha$  and  $E_\beta$  using the ordered references  $R^-$  and  $R^+$ .

In [8], the references were automatically computed as the global pseudo-extrema on each principal component determined on the entire color distribution of the image. In this way, three pairs of references were obtained:  $(\mathcal{R}_1^-, \mathcal{R}_1^+)$ ,  $(\mathcal{R}_2^-, \mathcal{R}_2^+)$ ,  $(\mathcal{R}_3^-, \mathcal{R}_3^+)$ , with  $\mathcal{R}_i^- < \mathcal{R}_i^+$ ,  $i = \overline{1, 3}$ . The ordering of the references was performed by using their projections on the black-white axis of the color space. Thus the two pseudo-morphological operations, dilation and erosion, can be defined for a color image  $f$  and a structuring element  $g$  having the support  $\mathcal{D}_g$ :

$$\begin{aligned}
 [\varepsilon_g(f)](x) &= \bigwedge_{z \in \mathcal{D}_g} f(x+z) \triangleq \\
 &= \begin{cases} \arg \min_i [\overrightarrow{\mathcal{R}_0^- \mathcal{R}_0^+} \cdot \overrightarrow{\mathcal{R}_0^- i}], i \in \{E_\alpha, E_\beta\} \\ \arg \min_i [\overrightarrow{\mathcal{R}_1^- \mathcal{R}_1^+} \cdot \overrightarrow{\mathcal{R}_1^- i}], i \in \{E_\alpha, E_\beta\} \text{ if } \overrightarrow{\mathcal{R}_0^- \mathcal{R}_0^+} \cdot \overrightarrow{E_\alpha E_\beta} = 0 \\ \arg \min_i [\overrightarrow{\mathcal{R}_2^- \mathcal{R}_2^+} \cdot \overrightarrow{\mathcal{R}_1^- i}], i \in \{E_\alpha, E_\beta\} \text{ if } \overrightarrow{\mathcal{R}_0^- \mathcal{R}_0^+} \cdot \overrightarrow{E_\alpha E_\beta} = \overrightarrow{\mathcal{R}_1^- \mathcal{R}_1^+} \cdot \overrightarrow{E_\alpha E_\beta} = 0 \end{cases} \quad (15)
 \end{aligned}$$

$$\begin{aligned}
 [\delta_g(f)](x) &= \bigvee_{z \in \mathcal{D}_g} f(x-z) \triangleq \\
 &= \begin{cases} \arg \max_i [\overrightarrow{\mathcal{R}_0^- \mathcal{R}_0^+} \cdot \overrightarrow{\mathcal{R}_0^- i}], i \in \{E_\alpha, E_\beta\} \\ \arg \max_i [\overrightarrow{\mathcal{R}_1^- \mathcal{R}_1^+} \cdot \overrightarrow{\mathcal{R}_1^- i}], i \in \{E_\alpha, E_\beta\} \text{ if } \overrightarrow{\mathcal{R}_0^- \mathcal{R}_0^+} \cdot \overrightarrow{E_\alpha E_\beta} = 0 \\ \arg \max_i [\overrightarrow{\mathcal{R}_2^- \mathcal{R}_2^+} \cdot \overrightarrow{\mathcal{R}_1^- i}], i \in \{E_\alpha, E_\beta\} \text{ if } \overrightarrow{\mathcal{R}_0^- \mathcal{R}_0^+} \cdot \overrightarrow{E_\alpha E_\beta} = \overrightarrow{\mathcal{R}_1^- \mathcal{R}_1^+} \cdot \overrightarrow{E_\alpha E_\beta} = 0 \end{cases} \quad (16)
 \end{aligned}$$

where  $\overrightarrow{\mathcal{R}_i^- \mathcal{R}_i^+}$  is the ordered direction determined the references  $\mathcal{R}_i^-$  and  $\mathcal{R}_i^+$ , and  $E_\alpha$  and  $E_\beta$  represent the local pseudo-extrema of the colors within the support of the structuring element. In Figure 9 several results using the PPM approach on the "Miro" image are presented. All operations were applied in RGB color space, since its components are highly correlated and thus using PCA makes sense.

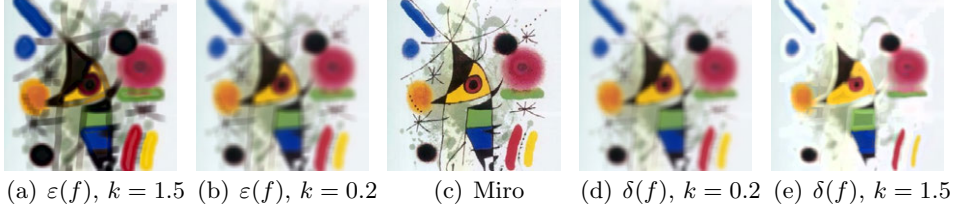


Fig. 9: Pseudo-erosion and dilation for "Miro" image using a flat structuring element of size  $11 \times 11$  and two values for the parameter  $k$ .

A similarity between the color and gray-scale approaches can be noticed: (i) the pseudo-dilations make the image lighter, while pseudo-erosions make it darker, as a consequence of using the black-white axis for ordering the reference colors; (ii) a low-pass filtering effect is introduced, intrinsic to the statistical process being used; (iii) the influence of the parameter  $k$  value of the Chebyshev inequality is similar: a small value determines a results similar to a smoothing filter, while a large value determines a non-linear behavior.

In [12] we proposed a pseudo-morphology based on the maximum distance computed for the vector values of the pixels within a neighborhood<sup>12</sup>. Given an image represented in the CIE Lab color space,  $f : \mathcal{D}_f \rightarrow \mathbb{R}^3$ , with the support  $\mathcal{D}_f \subset \mathbb{Z}^2$ , we define the two pseudo-extrema in the support  $\mathcal{D}_g$  of the flat structuring element  $g$  as:

$$\{\mathbf{e}_a, \mathbf{e}_b\} = \arg \max_{f(i), f(j)} d(f(i), f(j)), \quad \forall i, j \in \mathcal{D}_f \cap \mathcal{D}_g \quad (17)$$

where  $d(\cdot, \cdot)$  represents the CIE Lab  $\Delta E$  distance [37]. After choosing the two pseudo-extrema for the local window, the issue of labeling them can be solved based on distances to the black-white axis or to reference or convergence colors [7] [8]. We chose a lexicographic ordering  $<_\ell$ . For two vectors  $\mathbf{v}$  and  $\mathbf{v}'$ :

$$\forall \mathbf{v}, \mathbf{v}' \in \mathbb{R}^n, \mathbf{v} <_\ell \mathbf{v}' \Leftrightarrow \exists i \in \{1, \dots, n\}, (\forall j < i, v_j = v'_j) \wedge (v_i < v'_i) \quad (18)$$

We thus define the *pseudo-erosion* as the minimum, in the lexicographical sense:

$$[\varepsilon_g(f)](k) = \min_\ell \{\mathbf{e}_a, \mathbf{e}_b\} \quad \forall k \in \mathcal{D}_f \quad (19)$$

and the *pseudo-dilation* as the lexicographic maximum:

<sup>12</sup>R. Coliban, M. Ivanovici, Color and Multispectral Texture Characterization Using Pseudo-Morphological Tools, IEEE International Conference on Image Processing (ICIP), Paris, France, October 27-30, 2014, <http://dx.doi.org/10.1109/ICIP.2014.7025126>

$$[\delta_g(f)](k) = \max_{\ell} \{ \mathbf{e}_a, \mathbf{e}_b \} \quad \forall k \in \mathcal{D}_f \quad (20)$$

For multispectral images  $f : \mathcal{D}_f \rightarrow \mathbb{R}^n$ , we use the same definition for the pseudo-extrema, with the distance measure now representing the Euclidean distance in  $\mathbb{R}^n$ , with the labeling performed based on a pre-ordering of the pixel energy (the lexicographic ordering would have no relevance):

$$\forall \mathbf{v}, \mathbf{v}' \in \mathbb{R}^n, \mathbf{v} <_e \mathbf{v}' \Leftrightarrow \sum_{i=1}^n v_i^2 < \sum_{i=1}^n v'_i{}^2 \quad (21)$$

Figure 10 shows the results of using the pseudo-dilation operator based on maximum distance for various sizes of the structuring element for an image (Pompoms) in the data-base CAVE<sup>13</sup>, Columbia University, New York.



Fig. 10: Pseudo-dilations of image Pompoms for various sizes of the structuring element:  $3 \times 3$ ,  $5 \times 5$ ,  $7 \times 7$ ,  $9 \times 9$ .

As a direct application for texture analysis, for the Pompoms image we computed the granulometry and the morphological covariance for the multispectral case, according to the definitions in Chapter 4 of the present thesis (Figure 11) and we compared them with the ones computed for color and gray-scale versions of the same image: the evolution of all three curves are very similar, proving the validity of the operators extension to the multispectral domain.

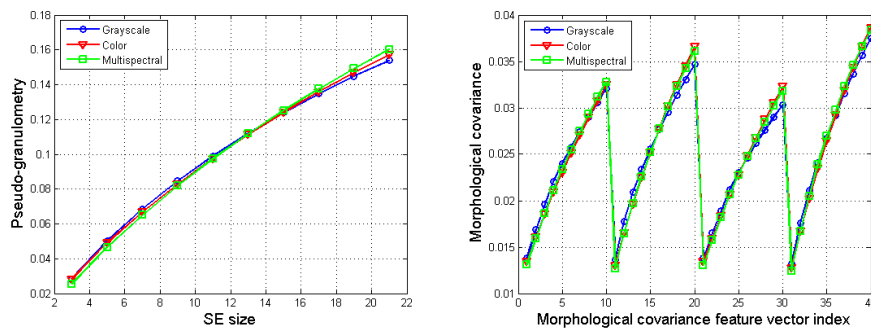


Fig. 11: Pseudo-granulometry and morphological covariance based on maximum distance.

<sup>13</sup><http://www.cs.columbia.edu/CAVE/databases/multispectral/>

## Applications

In what follows we shall focus on a major application - image segmentation, including an approach based on texture classification. The theoretical concepts of segmentation approaches are presented in works such [23] and [15]. We present briefly several segmentation techniques which are presented together with other approaches in the chapter entitled *Color Image Segmentation*<sup>14</sup> published in Springer.

### Watershed segmentation

The watershed segmentation technique is a region-based approach, where the image is modeled as a landscape [5] [35]. The approach is fundamentally linked to mathematical morphology. The segmentation process is inspired by natural phenomena (i.e. precipitation) - the rain falling on the image landscape will gradually flood the valleys and form basins; the dams between them will constitute the borders of the segments within the segmentation maps [6]. When the landscape is completely flooded, the *watersheds* give the segmentation map. In Figure 12 the segmentation process is illustrated: a) the considered basins begin to flood, then the basins  $V_1$  and  $V_3$  flood two local minima; b) a dam is built between valleys  $V_1$  and  $V_2$  and another one between  $V_2$  and  $V_3$ .

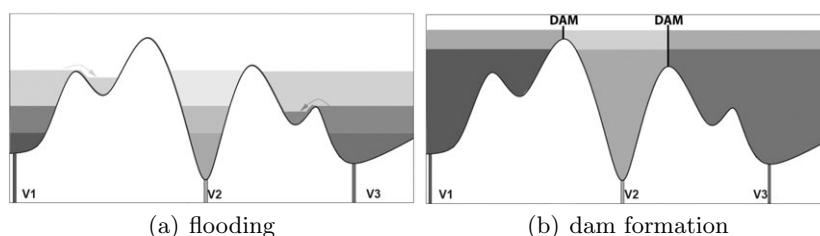


Fig. 12: Illustration of the watershed segmentation technique.

The watershed approach is traditionally applied in the original image domain, but there are approaches like [42] where the segmentation is performed in a feature space. In Figure 13 we show an example of watershed segmentation, using a local window of size  $21 \times 21$ . Usually a merging phase follows, in case of over-segmentation.

Chanussot et al. extended the watershed segmentation to the color domain using a bit mixing technique for multivalued morphology [10].

<sup>14</sup>M. Ivanovici, N. Richard, D. Paulus, *Color Image Segmentation*, in *Advanced Color Image Processing and Analysis*, ed. Christine Fernandez-Maloigne, Springer New York, 2013, ISBN 978-1-4419-6190-7, <http://www.springer.com/us/book/9781441961891>

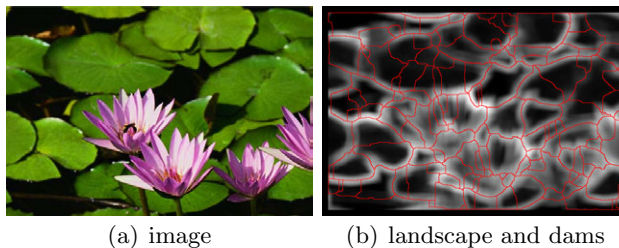


Fig. 13: Exemple of watershed segmentation.

### Active contours

The active contours, also known as *snakes*, were introduced by Terzopoulos et al. in 1988 [24] and are successfully used for image segmentation. They are defined as energy-minimizing splines guided by external constraint forces and influenced by image forces that pull it towards features such as edges.

The initial contour is incrementally deformed according to several specified energies. According to the original definition, an active contour is a spline  $c(s) = [x(s), y(s)]$ , with  $s \in [0, 1]$ , that minimizes the following energy functional [39]:

$$\varepsilon(c) = \varepsilon_{\text{int}}(c) + \varepsilon_{\text{ext}}(c) = \int_0^1 [E_{\text{int}}(c(s)) + E_{\text{ext}}(c(s))] ds \quad (22)$$

where  $\varepsilon_{\text{int}}(c)$  represents the *internal* energy, intrinsic to the spline, and  $\varepsilon_{\text{ext}}(c)$  the *external* energy, computed based on the image. The internal energy  $\varepsilon_{\text{int}}$  is usually:

$$\varepsilon_{\text{int}}(c) = \int_0^1 \frac{1}{2} [\alpha(s) |c'(s)|^2 + \beta(s) |c''(s)|^2] ds \quad (23)$$

where  $c'(s)$  and  $c''(s)$  are the first and the second derivatives, weighted by  $\alpha(s)$  and  $\beta(s)$ , which are usually considered to be constants in most implementations.

The external energy is given by a certain diffusion model. For extending the snakes to the color domain, we used the first order moment of the correlation integral to define a diffusion model for color images [21]. In Figure 14 we show results of our multi-scale approach. The hypothesis that is made is that in such images there are two types of textures, exhibiting different complexities: one corresponding to the salient object and the other to the background (the complexity of the latter one being usually smaller).

The external energy is linked to the correlation dimension (practically being the mean value of the  $C(\delta)$  distribution) and it represents a measure of the heterogeneity in a certain neighborhood, at a given resolution. The external energy forces that drive the active contours are given by the average

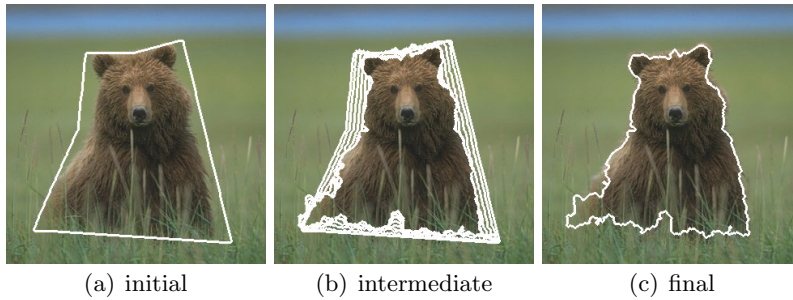


Fig. 14: Example of segmentation using active contours on an image from Berkeley data base (100080).

CIE Lab  $\Delta E$  distance computed locally at different resolutions<sup>15</sup>, based on the original image (see Figure 15). For a certain resolution, the value of one point  $(x, y)$  in the energetic surface is given by the average of  $n^2(n^2 - 1)/2$  distances in a neighborhood of size  $n \times n$  centered in that specific point.

$$E_{\text{ext}}(x, y)|_{n \times n} = \frac{2}{n^2(n^2 - 1)} \sum_{i=1}^{n^2} \sum_{j=i+1}^{n^2} \Delta E(v_i, v_j) \quad (24)$$

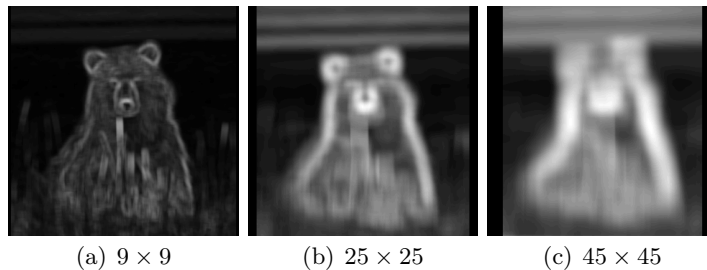


Fig. 15: Diffusion pseudo-images for Berkeley image 100080.

### Feature-based image segmentation

Very often segmentation is performed in a feature space, not directly on the pixel data. Usually a classification technique is used (e.g. k-means) to classify the pixels according to local features computed within a certain vicinity around it. In Figure 16 we show the results of segmentation based on the two morphological features presented in Chapter 4: the granulometry and the morphological covariance. The classification was unsupervised,  $k$ -means for  $k = 2$  based on the hypothesis that there are only two regions in

<sup>15</sup>M. Ivanovici, D. Stoica, Color diffusion model for active contours - an application to skin lesion segmentation, Annual International Conference of the IEEE, Engineering in Medicine and Biology Society (EMBC), 2012, <http://dx.doi.org/10.1109/EMBC.2012.6347202>

the image, from the point of view of texture characterization: the object of interest and the background.

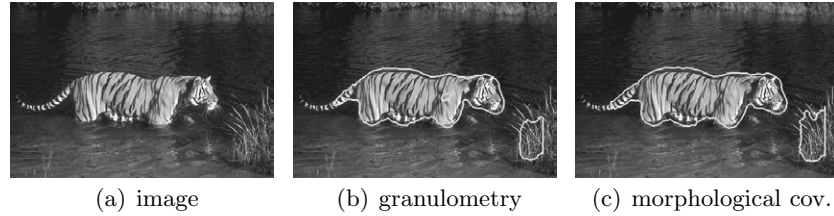


Fig. 16: Example of segmentation using local morphological features.

To illustrate this color textured image segmentation technique, we used as local texture feature the vector of volumes computed between pseudo-dilation and pseudo-erosion, for varying sizes of the structuring element. The two pseudo-morphological operations are presented in Chapter 4 of the thesis. We compare the results of our approach with two approaches: the  $\alpha$ -trimmed pseudo-morphology, computed in the RGB color space and with the lexicographical morphological approach, using the HSV color space with (V,S,H) component priority. We computed the vector of the local volume, using a sliding window, followed by a  $k$ -means classification in two classes. We also generated a ground-truth segmentation, performed by a human, which is used as a reference for computing the percentage of the correctly classified pixels. The results are presented in Figure 17.

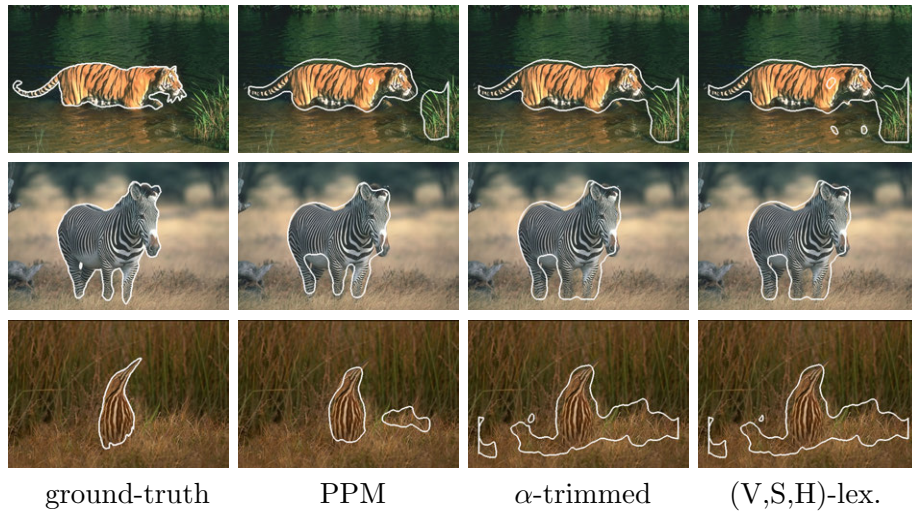


Fig. 17: Segmentation results using color texture features.

As a quantitative comparison, we computed the percentage of correctly classified pixels as a segmentation evaluation criterion, as in [9]. The results

are presented in the table below. In most of our experiments, PPM leads to a better segmentation, proving the increased ability to capture the complexity of textures and its variation along the analysis scales.

	PPM	$\alpha$ -trimmed	(V,S,H) lex.
Berkeley108073	<b>92.37%</b>	91.41%	90.57%
Berkeley130066	<b>96.06%</b>	95.37%	95.40%
Berkeley43033	<b>96.35%</b>	86.01%	86.19%

### Instead of conclusions

The segmentation process requires addressing three issues: (i) the features capturing the homogeneity of regions, (ii) the similarity measures or distance functions between features content and (iii) the segmentation framework which optimizes the segmentation map as a function of the feature-metric pair. We presented the color segmentation frameworks separately, but very often there is only a fine frontier between them and quite often hybrid techniques emerge, that combine for instance pyramids and watersheds [1]. However, the segmentation approaches evolved towards unanimously-accepted frameworks: pyramidal approaches, watershed, JSEG, graph cuts, normalized cuts, active contours or more recently, TurboPixels.

Nowadays the question still remains since Haralick: which is the best value for the parameters of the homogeneity criteria? There are no recommended recipes. New perspectives come from psychophysics with perceptual theory, in particular Gestalt theory. As the homogeneity or heterogeneity definition have been expressed as complexity of a feature distribution, these perceptual theories search to explain what are the physical parameters that are taken into account by the human visual system. An open question is given by the relationship between the similarity law from Gestalt theory and the homogeneity. Randall in [34] links the similarity law to grouping into homogeneous regions of color or texture. Nevertheless, the definition of homogeneity and implicitly the one of complexity is still imperfect, and represents a niche for the future research.



# Bibliography

- [1] J. Angulo. *Morphologie mathématique et indexation d'images couleur. Application à la microscopie en biomédecine*. Centre de Morphologie Mathématique, Ecole des Mines de Paris, France, 2003.
- [2] J. Angulo. Pseudo-morphological image diffusion using the counter-harmonic paradigm. In J. Blanc-Talon, D. Bone, W. Philips, D. Popescu, and P. Scheunders, editors, *Advanced Concepts for Intelligent Vision Systems*, volume 6474 of *Lecture Notes in Computer Science*, pages 426–437. Springer Berlin Heidelberg, 2010.
- [3] E. Aptoula and S. Lefèvre. A comparative study on multivariate mathematical morphology. *Pattern Recognition*, 40(11):2914–2929, November 2007.
- [4] V. Barnett. The ordering of multivariate data. *Journal of the Royal Statistical Society*, 139(3):318 – 355, 1976.
- [5] S. Beucher. Watersheds of functions and picture segmentation. *Acoustics, Speech, and Signal Processing, IEEE International Conference on ICASSP '82.*, 7:1928 – 1931, may 1982.
- [6] S Beucher. Watershed, hierarchical segmentation and waterfall algorithm. In J Serra and P Soille, editors, *Mathematical Morphology And Its Applications To Image Processing*, volume 2 of *Computational Imaging And Vision*, pages 69–76, 1994.
- [7] A Caliman, M. Ivanovici, and N. Richard. Probabilistic pseudo-morphology for greyscale and color images. *Pattern Recognition*, 47(2):721 – 735, 2014.
- [8] A Caliman, M. Ivanovici, N. Richard, and G. Toacse. A multivariate mathematical morphology based on orthogonal transformation, probabilistic extrema estimation and distance optimization. In C. L. Hendriks, G. Borgefors, and R. Strand, editors, *Mathematical Morphology and Its Applications to Signal and Image Processing*, volume 7883 of *Lecture Notes in Computer Science*, pages 255–266. Springer Berlin Heidelberg, 2013.

- 
- [9] A. Carleer, O. Debeir, and E. Wolff. Assessment of very high spatial resolution satellite image segmentations. *Photogrammetric Engineering and Remote Sensing*, 71(11):1285–1294, 2005.
- [10] J. Chanussot and P. Lambert. Total ordering based on space filling curves for multivalued morphology. In *Proceedings of the 4th international symposium on Mathematical morphology and its applications to image and signal processing*, ISMM '98, pages 51–58, Norwell, MA, USA, 1998. Kluwer Academic Publishers.
- [11] P. Chebyshev. Des valeurs moyennes. *Journal de mathematiques pures et appliquees*, 2(12):177–184, 1867.
- [12] R.-M. Coliban and M. Ivanovici. Color and multispectral texture characterization using pseudo-morphological tools. In *Image Processing (ICIP), 2014 IEEE International Conference on*, pages 630–634, Oct 2014.
- [13] G.R. Cross and A.K. Jain. Markov random field texture models. *IEEE Transactions on Pattern Analysis and Machine Intelligence*, PAMI(1):25–39, 1983.
- [14] K. Falconer. *Fractal Geometry, mathematical foundations and applications*. John wiley and Sons, 1990.
- [15] Rafael C. Gonzalez and Richard E. Woods. *Digital Image Processing (3rd Edition)*. Prentice-Hall, Inc., Upper Saddle River, NJ, USA, 2006.
- [16] J. Goutsias and H. J. A. M. Heijmans. Fundamenta morphologicae mathematicae. *Fundamenta Informaticae - Special issue on mathematical morphology*, 41(1-2):1–31, January 2000.
- [17] A. Hanbury and J. Serra. Morphological operators on the unit circle. *IEEE Transactions on Image Processing*, 10(12):1842–1850, 2001.
- [18] R. Haralick, K. Shanmugam, and I. Dinstein. Textural feature for image classification. In *IEEE Transactions on System Man and Cybernetics*, volume 3(6), pages 610–621, November 1973.
- [19] M. Ivanovici, A. Caliman, N. Richard, and C. Fernandez-Maloigne. Towards a multivariate probabilistic morphology for colour images. In *Proceedings of the 6th European Conference on Colour in Graphics, Imaging and Vision*, pages 189 – 193, Amsterdam, the Netherlands, May 6-9 2012.
- [20] M. Ivanovici and N. Richard. Fractal dimension of colour fractal images. *IEEE Transactions on Image Processing*, 20(1):227–235, January 2011.

- 
- [21] M. Ivanovici and D. Stoica. Color diffusion model for active contours - an application to skin lesion segmentation. In *Engineering in Medicine and Biology Society (EMBC), 2012 Annual International Conference of the IEEE*, pages 5347–5350, Aug 2012.
- [22] A.K. Jain and F. Farrokhnia. Unsupervised texture segmentation using gabor filters. In *Systems, Man and Cybernetics, 1990. Conference Proceedings., IEEE International Conference on*, pages 14–19, 1990.
- [23] Anil K. Jain. *Fundamentals of digital image processing*. Prentice-Hall, Inc., Upper Saddle River, NJ, USA, 1989.
- [24] Michael Kass, Andrew Witkin, and Demetri Terzopoulos. Snakes: Active contour models. *International Journal of Computer Vision*, 1(4):321–331, 1988.
- [25] J.M. Keller and S. Chen. Texture description and segmentation through fractal geometry. *Computer Vision, Graphics and Image processing*, 45:150–166, 1989.
- [26] K.I. Laws. Rapid texture identification, 1980.
- [27] B.B. Mandelbrot. *The Fractal Geometry of Nature*. W.H. Freeman and Co, New-York, 1982.
- [28] G. Matheron. *Random sets and integral geometry*. John Wiley and Sons, Inc., 1975.
- [29] T. Ojala, T. Mäenpää, M. Pietikäinen, J. Viertola, J. Kyllönen, and S. Huovinen. Outex - new framework for empirical evaluation of texture analysis algorithms. In *Proceedings of the 16th International Conference on Pattern Recognition - Volume 1, ICPR02*, Washington, DC, USA, 2002. IEEE Computer Society.
- [30] A. Papoulis. *Probability, random variables, and stochastic processes*. McGraw-Hill, 3rd edition, 1991.
- [31] K. Pearson. On lines and planes of closest fit to systems of points in space. *Philosophical Magazine*, 2(6):559–572, 1901.
- [32] H.O. Peitgen and D. Saupe. *The sciences of fractal images*. Springer Verlag, 1988.
- [33] M. Petrou and P. G. Sevilla. *Image Processing: Dealing with Texture*. John Wiley and Sons, 2006.
- [34] J. Randall, L. Guan, W. Li, and X.Zhang. The hcm for perceptual image segmentation. *Neurocomputing*, 71(10-12):1966–1979, June 2008.

- 
- [35] Jos B.T.M. Roerdink and Arnold Meijster. The watershed transform: Definitions, algorithms and parallelization strategies. *Fundamenta Informaticae*, 41:187–228, 2001.
  - [36] J. Serra. *Image Analysis and Mathematical Morphology*, volume I. Academic Press, 1982.
  - [37] R. Seve. Practical formula for the computation of CIE 1976 hue difference. *Color Research and Application*, 21(4):314–314, 1996.
  - [38] P. Soille. *Morphological Image Analysis: Principles and Applications*. Springer-Verlag, 2002.
  - [39] D. Terzopoulos. Deformable models: Classic, topology-adaptive and generalized formulations. In S. Osher and N. Paragios, editors, *Geometric Level Set Methods in Imaging, Vision, and Graphics*, chapter 2, pages 21–40. Springer-Verlag, New York, 2003.
  - [40] M. Tuceryan and A. K. Jain. Texture analysis. In *The Handbook of Pattern Recognition and Computer Vision*, pages 207–248. World Scientific Publishing Co., 1998.
  - [41] R. Voss. Random fractals : characterization and measurement. *Scaling phenomena in disordered systems*, 10(1):51–61, 1986.
  - [42] Yu-Jin Zhang. *Advances in Image and Video Segmentation*. IRM Press, 2006.